

# A Joint Visual Compression and Perception Framework for Neurlomorphic Spiking Camera

Kexiang Feng, Chuanmin Jia, Siwei Ma, *Fellow, IEEE*, and Wen Gao, *Fellow, IEEE*

**Abstract**—The advent of neurlomorphic spike cameras has garnered significant attention for their ability to capture continuous motion with unparalleled temporal resolution. However, this imaging attribute necessitates considerable resources for binary spike data storage and transmission. In light of compression and spike-driven intelligent applications, we present the notion of Spike Coding for Intelligence (SCI), wherein spike sequences are compressed and optimized for both bit-rate and task performance. Drawing inspiration from the mammalian vision system, we propose a dual-pathway architecture for separate processing of spatial semantics and motion information, which is then merged to produce features for compression. A refinement scheme is also introduced to ensure consistency between decoded features and motion vectors. We further propose a temporal regression approach that integrates various motion dynamics, capitalizing on the advancements in warping and deformation simultaneously. Comprehensive experiments demonstrate our scheme achieves state-of-the-art (SOTA) performance for spike compression and analysis. We achieve an average 17.25% BD-rate reduction compared to SOTA codecs and a 4.3% accuracy improvement over SpiReco for spike-based classification, with 88.26% complexity reduction and 42.41% inference time saving on the encoding side.

**Index Terms**—Spike compression, visual intelligence, end-to-end spike coding.

## I. INTRODUCTION

THE surge in autonomous driving, UAV technologies, and intelligent city strategies has intensified the demand for scene capture and imaging of ultra-high motion dynamics. These applications operate in high-speed environments, requiring a high temporal resolution to enable high-frame rate imaging and real-time identification, posing a significant challenge for traditional cameras. The target object must remain stationary during the rolling shutter scanning period to avoid motion blur and structural distortion [1]. Furthermore, due to the synchronous imaging principle of the device, there may be instances where certain content or information occurring between two successive shots may not be accurately recorded [2]. These limitations fail to meet the specific requirements of the aforementioned applications [3] [4].

K. Feng is with Institute of Computing Technology, Chinese Academy of Sciences, Beijing 100190, China, with the University of Chinese Academy of Sciences, Beijing 100049, China, and also with the National Engineering Research Center of Visual Technology, Peking University, Beijing 100871, China (e-mail: fengkexiang21@mails.ucas.ac.cn).

C. Jia is with the Wangxuan Institute of Computer Technology, Peking University, Beijing 100080, China (email: cmjia@pku.edu.cn).

S. Ma and W. Gao are with the National Engineering Research Center of Visual Technology, Peking University, Beijing 100871, China (email: {swma, wgao}@pku.edu.cn).

Correspondence to: Chuanmin Jia.

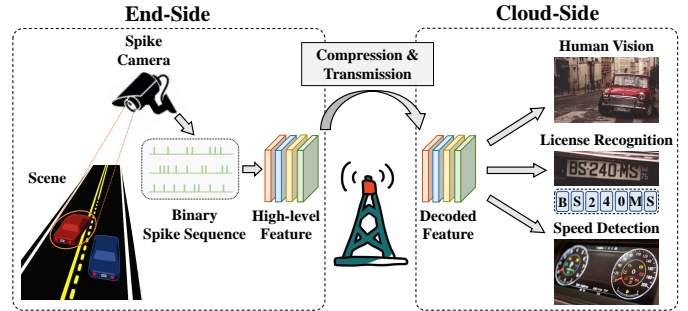


Fig. 1. Sketch for application of spike vision. At the end-side, spike camera captures scenes and generates binary spike sequences, which are extracted as high-level features. After compression and transmission, decoded features are utilized for several applications at the cloud-side.

Drawing inspiration from the fovea of the mammalian retina [5] [6], a groundbreaking spike camera has been introduced to overcome these limitations [7]. Spike cameras, by asynchronously recording luminance intensity through spike firing, transcend the constraints of traditional exposure methods. This imaging principle affords an ultra-high temporal resolution of 10kFPS, effectively addressing motion blur and content loss in high-speed scenarios. Such capabilities enable numerous applications with end-cloud collaboration [8] [9], as depicted in Fig. 1. Scenes are captured and converted into spikes, which are then extracted into features at the end-side. These features undergo compression and transmission, followed by decoding and analysis for various intelligent applications such as scene reconstruction, license recognition, and speed detection. However, the ultra-high temporal resolution leads to a significant increase in data volume, exacerbating challenges in storage and transmission. For instance, a spike camera with a spatial resolution of  $1k \times 1k$  and a temporal resolution of 40k generates data at a rate that can impose a significant burden on bandwidth, reaching up to 40Gbps. Thus, the development of an efficient compression method for spike data is of paramount importance.

By comprehensively considering the imaging principles of spike cameras and the relationship between spike data and intelligent applications, we introduce a novel compression framework specifically tailored for spike data. Our framework comprises three key components: short-term feature extraction, feature compression, and long-term feature analysis. Through joint optimization, spike sequences are encoded with minimal bit usage, achieving optimal performance for downstream tasks simultaneously. The major contributions of this paper are summarized as follows:

- We conceptualize Spike Coding for Intelligence (SCI), which considers compression efficiency and the performance of spike-based analysis comprehensively. We further propose a novel spike compression framework based on the *compress-and-analyze-simultaneously* (CAAS) paradigm. By end-to-end optimization, our scheme realizes state-of-the-art (SOTA) performance in both compression and intelligent analysis tasks, establishing a new direction for collaborative spike intelligence.
- Drawing inspiration from mechanisms in mammalian vision, we propose a dual-pathway architecture to handle spatial semantics and motion information as distinct streams, which are then integrated through a Pathway Fusing Unit (PFU) to address challenges arising in both low and high-speed scenarios effectively. To preserve the content fidelity between decoded features and motion vectors, a Feature-level Motion Vector Refinement (FMVR) is introduced to constrain consistency. We further propose an Associated Feature Regression (AFR) approach incorporating different motion dynamics in the temporal domain, jointly leveraging the advances of warping and deformation. Ablation studies indicate that all technological innovations we proposed yield good results.
- Extensive experiments demonstrate the superiority of our method over other approaches, achieving leading performance for intelligent applications at both pixel-level and semantic-level. For spike coding, our scheme rebuilds terrific scenes with transmitting minimal bits, reaching a **17.25%** BD-rate reduction and obtaining superior subjective quality. For spike classification, our method accomplishes high accuracy for datasets S-MNIST, S-CIFAR, and S-CALTECH, exceeding the SOTA method by **0.5%**, **2.5%**, and **4.3%** respectively.

## II. RELATED WORK

We comprehensively review related work on spike processing, including spike analysis and compression. There is a growing trend of spike-based intelligent applications becoming increasingly popular due to their excellent performance, making spike compression particularly important.

**Spike Analysis.** This includes pixel-level scene reconstruction and semantic-level classification. For reconstruction, the scene is estimated from the average spike firing rate within sliding windows, which can hardly handle the rapid change of light intensity. To cope with this, Zhao *et al.* proposed a hierarchical structure to rebuild scenes progressively [10]. Based on multi-stage motion estimation and temporal fusion, artifacts and distortion are effectively decreased. Furthermore, the structure of the mammalian retina was mimicked for processing visual signals, though this proved challenging. For classification, spatial information is supervised by motion characteristics, resulting in better accuracy. Binary modulation is introduced to reduce computational consumption, diminishing complexity while maintaining performance [11]. To further utilize the spatio-temporal correlation within spikes, a transformer-like architecture was proposed for optimizing global association [12].

**Spike Compression.** Simulating conventional codecs, which are based on partition and prediction, spike sequences were divided into several overlapped voxels [13] and compressed respectively. To utilize the correlation between spikes effectively, inter-voxel reference was introduced to achieve better performance. Breaking the limitation of binary data format, spikes with discrete values were converted to continuous inter-spike intervals, providing a prerequisite for NN-based compression. Feng *et al.* proposed an end-to-end learnable framework [14], which decouples the spike compression problem into scene construction plus scene coding tasks, achieving great performance in information fidelity. Dong *et al.* addressed the challenges of lossless compression for continuous spike streams and introduced a learned compression model [15], achieving state-of-the-art performance.

**Neural Video Compression.** With the emergence of deep learning, neural video compression (NVC) methods have evolved rapidly, leading to significant advancements in the field [16] [17] [18]. DVC [19] pioneered the first fully neural video compression framework, which replaced traditional optical flow estimation and residual coding modules with trainable neural networks optimized through a rate-distortion loss function. Subsequently, DCVC [20] leveraged feature-domain contexts as conditions, enabling both encoder and decoder to access rich information for reconstructing high-frequency content, thereby enhancing video quality. Building upon DCVC, DCVC-DC [21] introduced hierarchical quality patterns across frames to enrich long-term, high-quality temporal contexts and employs a group-based offset diversity mechanism for improved temporal context mining. Additionally, a quadtree-based partitioning strategy is utilized to enhance spatial context diversity during latent representation encoding.

## III. PROBLEM FORMULATION

### A. Principles of Spike Generation

The spike camera is composed of two-dimensional photosensitive array, which simulates the fovea structure of retina. Different from event-based cameras, the spike camera accumulates photons at each position and generates spikes through an integrate-and-fire ( $\mathcal{IF}$ ) process. This can be formulated as

$$S_t, v_t = \mathcal{IF}(v_{t-1}, I_t), \quad (1)$$

where  $v_{t-1}$  and  $v_t$  represent membrane potential at moment  $t-1$  and  $t$ , while  $I_t$  and  $S_t$  indicate luminance and spike at moment  $t$  respectively. By iterating Eq. 1, the spike sequence  $\{S_t\}$  is generated as following

$$\{S_t\} = \mathcal{IF}[v_0, \{I_t\}], \quad (2)$$

where  $v_0$  represents the initial membrane potential and  $\{I_t\}$  denotes the luminance sequence. As a matter of fact, pixels in brighter environment can reach threshold faster and thus can fire spikes more frequently. This observation aligns with the biological perspective.

The  $\mathcal{IF}$  process motioned above can be separated into three steps. The intensity of illumination  $I_t$  integrates on membrane potential  $v_t$ , subsequently determining the spike  $s_t$  based on

TABLE I  
SIMILARITIES AND DIFFERENCES BETWEEN EVENT AND SPIKE CAMERA.

	Imaging Mechanism	Temporal Resolution	Data Structure	Value Range	Condition for Generation
Event Camera	asynchronous imaging	ultra-high	set of $(x, y, t, p)$	1 or -1	$\ln(I(t + \Delta t)) - \ln(I(t)) = p\theta$
Spike Camera			tensor with size of $H \times W \times T$	1 or 0	$\alpha \int_t^{t+\Delta t} I(\tau) d\tau = \theta$

whether  $v_t$  surpasses threshold  $\theta$ . Finally,  $v_t$  undergoes a reset according to  $s_t$ . These three steps can be formalized as

$$v_t = v_{t-1} + \alpha I_t, \quad (3)$$

$$S_t = \begin{cases} 1, & v_t \geq \theta \\ 0, & \text{otherwise} \end{cases}, \quad (4)$$

$$v_t = \begin{cases} (1 - S_t)v_t, & \text{hard scheme} \\ v_t - S_t\theta, & \text{soft scheme} \end{cases}, \quad (5)$$

where  $\alpha$  represents photoelectric conversion efficiency.

We further provide a detailed comparison of the similarities and differences between event and spike camera in terms of imaging principles and data characteristics, as shown in Table I.

### B. Theory Conceptualization

Differing from images and videos, which are visually interpretable for humans, spike data encapsulates scenes in an abstract manner and is not inherently designed for visual perception. This data format offers the advantage of enabling intelligent applications to be executed with high precision and low latency. Consequently, the primary objective in decoding spike data is to optimize performance for specific tasks, rather than striving for spike-level fidelity. To illustrate this characteristic, we introduce the concept of Spike Coding for Intelligence (SCI), which comprehensively considers compression efficiency and task performance.

Given task set  $\{T_i\}$ ,  $Y_i$  and  $\hat{Y}_i$  denote the ground truth and generated result from spike sequence  $\{S_t\}$  for task  $T_i$ . The goal of SCI is decreasing the code-length of bit stream for transmission while keeping fidelity between each  $Y_i$  and  $\hat{Y}_i$ . The loss function can be formulated as

$$\mathcal{L} = \mathcal{R}(\{S_t\}) + \sum_i \lambda_i \mathcal{D}_i(Y_i, \hat{Y}_i), \quad (6)$$

where  $\mathcal{R}$  denotes bit-rate estimation,  $\mathcal{D}_i$  and  $\lambda_i$  denotes distortion and weight for  $T_i$ .

### C. Paradigm Comparison

Referring to task-oriented compression frameworks [22] [23], we introduce three SCI paradigms as shown in Fig. 2. Green box denotes the encoding side, while blue represents the decoding side. For the *compress-then-analyze* (CTA) paradigm depicted in Fig. 2(a), spikes are first encoded into a bitstream and then decoded back to spikes, which are subsequently analyzed for downstream tasks. However, the extremely weak spatio-temporal continuity leads to poor efficiency in compression and noticeable distortion in reconstruction, which further

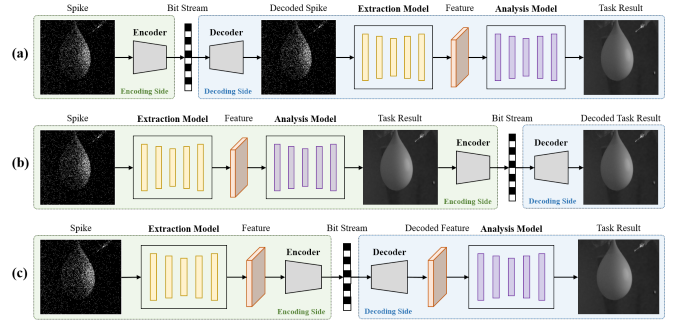


Fig. 2. Comparison between three paradigms for spike compression and analysis, including (a) *compress-then-analyze* (CTA), (b) *analyze-then-compress* (ATC) and (c) *compress-and-analyze-simultaneously* (CAAS) paradigms. Extensive experimental results show CAAS paradigm exceeds other two paradigms, providing a novel perspective for SCI.

results in inferior task performance. For the *analyze-then-compress* (ATC) paradigm depicted in Fig. 2(b), spikes are first analyzed for downstream tasks, and the analysis results are then compressed. Nevertheless, the results for the task may be unfriendly for compression, and the bitstream is not versatile enough for multiple tasks.

Considering compression efficiency, task performance, and bitstream versatility, we propose the *compress-and-analyze-simultaneously* (CAAS) paradigm depicted in Fig. 2(c). Spikes are first extracted into features, which are then compressed and analyzed for downstream tasks. On the one hand, the strong spatio-temporal correlation within features can be utilized to reduce the bit rate. On the other hand, features aggregate low-level semantic information, which can be repurposed in several high-level tasks. Extensive experiments demonstrate the superiority of the CAAS paradigm over the CTA and ATC paradigms, providing a novel perspective for SCI.

Given the limited computational capability at the end-side, which severely restricts the usage of spike cameras, our proposed CAAS paradigm is resource-efficient, making it more applicable to the end-cloud collaborative architecture. The electrical power limitation at the end-side (<10W) restricts its computational capability (<10GFLOPS), necessitating a simplification of the encoding procedure to reduce delay and avoid overheating. In contrast, the cloud-side has abundant computing resources (>100TFLOPS) and can offload complex computational operations. As such, we design the framework with lower complexity on the end side and higher complexity on the cloud side, achieving a balance between encoding and decoding based on the difference in end-cloud computing resources. The spike camera, serving as the end-side (edge device), converts spikes to features through an extraction model and then compresses them into a bitstream via an encoding

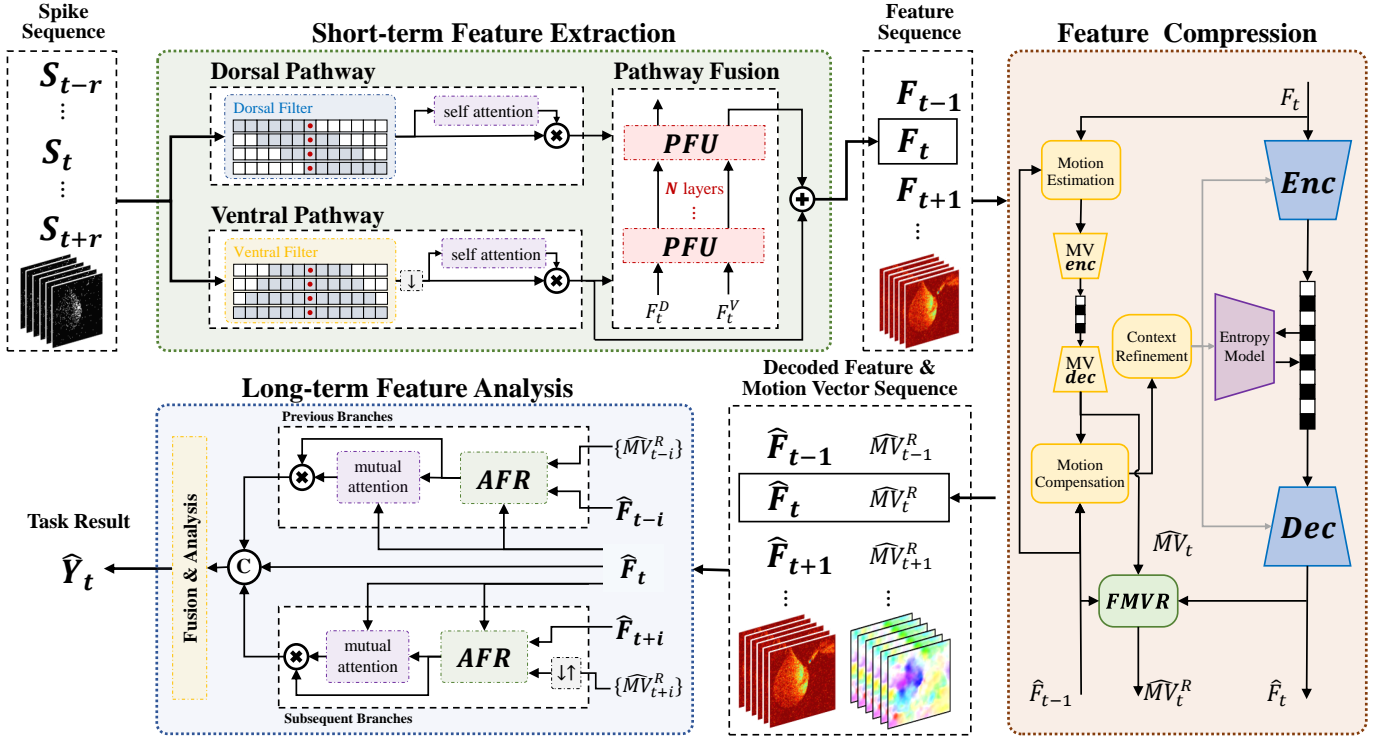


Fig. 3. Framework of method which compresses spike sequence and analyzes for downstream tasks simultaneously. The whole process is mainly separated into three modules. The short-term feature extraction module converts spike sequence into compression-friendly feature ( $F_t \in [0, 1]^{h \times w}$ ). The feature compression module effectively encodes feature sequence, eliminating intra- and inter-feature redundancies. The long-term feature analysis module optimizes for downstream task performance using decoded feature sequence and refined motion vector sequence.

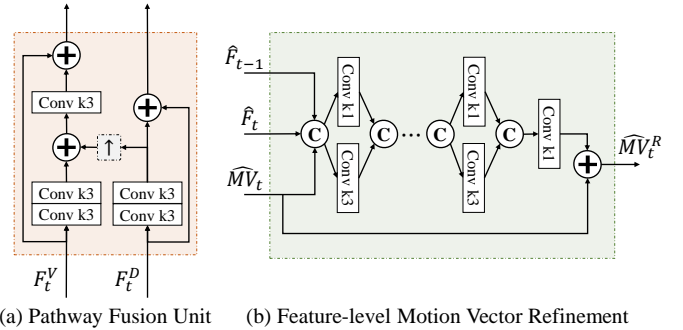
model. The cloud-side transforms the bitstream into features through a decoding model and applies them for intelligent applications by analysis models.

#### IV. METHODOLOGY

The overarching framework of our study is illustrated in Fig. 3, outlining a three-step process for the efficient compression of spike sequences and their subsequent analysis in downstream applications. Initially, the spike sequence  $\{S_t\}$  is transformed into a feature sequence  $\{F_t\}$ , which is amenable to coding. Subsequently,  $\{F_t\}$  undergoes effective compression, achieved by reducing both intra- and inter-feature redundancies. In the final step, we utilize the decoded feature sequence  $\{\hat{F}_t\}$  along with the refined motion vector sequence  $\{\hat{M}V_t^R\}$  to enhance performance in downstream tasks. Detailed explanations of our methodology are provided in the following subsections.

##### A. Short-term Feature Extraction

This module leverages the correlation in spike sequences  $\{S_t\}$  to amalgamate spatio-temporal data and formulate an efficient feature representation  $F_t$ . Inspired by the Two-streams Hypothesis [24] [25], which postulates the bifurcation of visual information into two distinct streams, we develop a dual-pathway architecture. The dorsal pathway focuses on motion characteristics, detecting positions and changes with the assistance of a sliding window-based temporal filter as shown in Fig. 5 (a). Conversely, the ventral pathway integrates



(a) Pathway Fusion Unit (b) Feature-level Motion Vector Refinement

Fig. 4. Detailed structure of (a) PFU and (b) FMVR. The PFU fuses spatial semantic information from dorsal pathway and motion characteristic from ventral pathway to generate features which are compression-friendly. The FMVR utilizes decoded features to constrain consistency of content between feature and latent domain.

spatial semantics and perceives structural information via a multi-scale temporal filter as shown in Fig. 5 (b). Both filters are binarized and enhanced by a self-attention mechanism submodule [26].

Emerging biological research indicates a symbiotic relationship between the dorsal and ventral streams, especially in processing detailed semantics [27] [28]. This observation prompts the creation of the Pathway Fusion Unit (PFU), which is depicted in Fig. 4(a). By employing  $N$  layers of PFUs, features from dorsal and ventral pathways are effectively collaborated, producing a feature  $F_t$  enriched with integrated spatio-temporal information and friendly for compression, as

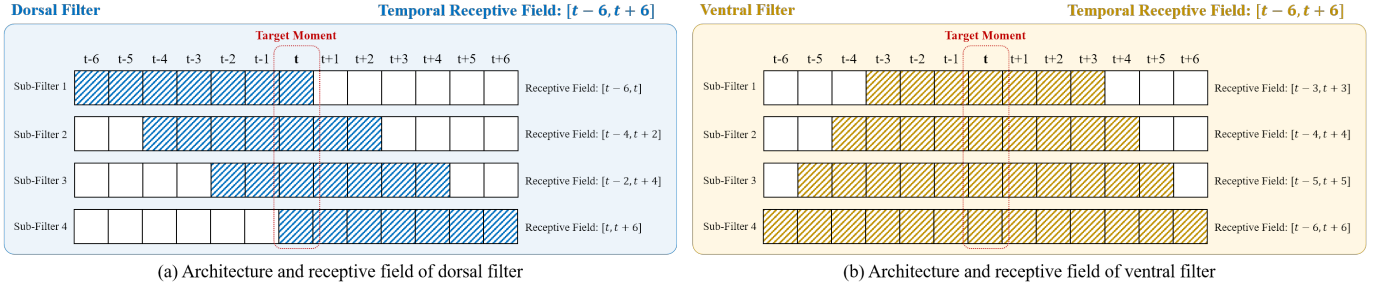


Fig. 5. Comparison of architecture and temporal receptive field between dual-pathway filters. The dorsal filter consists of sliding window-based temporal sub-filters, whereas the ventral filter comprises multi-scale temporal sub-filters.

formulated below:

$$F_t = \mathcal{P}\mathcal{F}U^{[N]}(F_t^D, F_t^V) + F_t^V, \quad (7)$$

where  $F_t^D$  and  $F_t^V$  denote features derived from the dorsal and ventral pathways, respectively.

### B. Feature Compression

This module employs advanced compression techniques to encode the feature sequence  $\{F_t\}$  into a compact bitstream while ensuring that the decoded feature sequence  $\{\hat{F}_t\}$  has minimal distortion. The architectural design closely resembles that of SOTA learning-based video codecs [19] [20] [21]. Initially,  $F_t$  and the preceding decoded feature  $\hat{F}_{t-1}$  are used to estimate the decoded motion vector  $\hat{M}V_t$ . Based on  $\hat{F}_{t-1}$  and  $\hat{M}V_t$ , contextual conditions for the encoder and decoder are established.  $F_t$  then undergoes encoding into a bitstream in the most compact form, which is decoded as  $\hat{F}_t$  with minimal distortion.

In conventional feature codecs,  $\hat{M}V_t$  is only used for decoding  $\hat{F}_t$  and will eventually become deprecated. We recognize that  $\hat{M}V_t$  encapsulates motion details between  $\hat{F}_{t-1}$  and  $\hat{F}_t$ , which can be invaluable for subsequent alignment. However,  $\hat{M}V_t$  only works in the latent domain, which is incompatible with feature contents [29]. Thus, we propose the Feature-level Motion Vector Refinement (FMVR), which is shown in Fig. 4(b). Composed of convolution layers with small kernels, FMVR focuses on local similarity and constrains content consistency between the feature and latent domains [30].

$$\hat{M}V_t^R = \mathcal{F}\mathcal{M}\mathcal{V}\mathcal{R}(\hat{M}V_t | \hat{F}_{t-1}, \hat{F}_t). \quad (8)$$

$\hat{M}V_t^R$  is then preserved to fully leverage motion information for alignment.

### C. Long-term Feature Analysis

This module regresses  $\{\hat{F}_t\}$  to moment  $t$  with the assistance of  $\{\hat{M}V_t^R\}$  and fuses them to generate the result  $\hat{Y}_t$  for the task. By aggregating abundant context, artifacts are effectively eliminated, and performance is significantly improved.  $\{\hat{F}_t\}$  and  $\{\hat{M}V_t^R\}$  are split into previous and subsequent branches, within which features are aligned separately. Traditional alignment methods predominantly rely on optical flow and assume that each pixel moves from only one previous location [31]

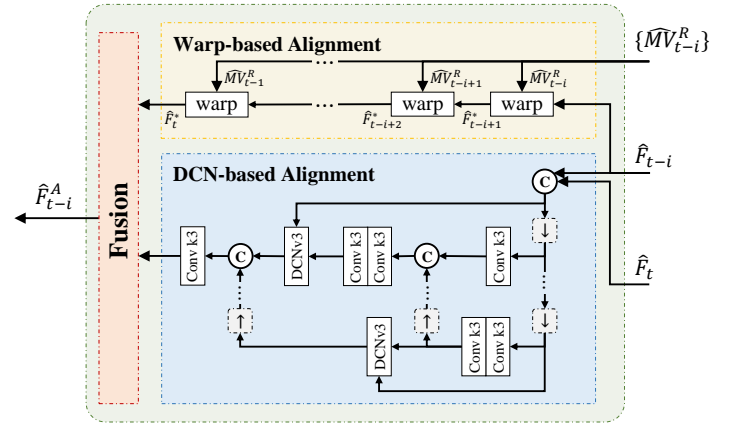


Fig. 6. Detailed structure of AFR, which incorporates different motion dynamics in temporal domain. Precise regressed feature is generated via leveraging the advances of warping and deformation approaches, which exhibits smoother transitions and leads to more accurate result for tasks.

[32], exhibiting limited diversity and imprecision at a fine-grained level. Recent advancements have leveraged the Deformable Convolution Network (DCN) [33] [34] to produce multiple groups of offsets and masks, enhancing sub-pixel level precision and fault tolerance [35] [36]. Nonetheless, DCN exhibits training instability, and its spatial receptive field is constrained in capturing large-scale motion [37]. Hence, we amalgamate both warping and deformation approaches, introducing the Associated Feature Regression (AFR) depicted in Fig. 6.

$$\hat{F}_{t-i}^A = \mathcal{A}\mathcal{F}\mathcal{R}(\hat{F}_t, \hat{F}_{t-i}, \{\hat{M}V_{t-i}^R\}), \quad (9)$$

where  $\hat{F}_{t-i}^A$  represents the aligned feature at moment  $t$ . Large-scale and small-scale motions are comprehensively captured, resulting in more precise alignment and superior fault tolerance. After alignment, preliminary results are generated and then fused to produce  $\hat{Y}_t$ . Experimental results demonstrate that our AFR outperforms both warping and deformation methods in feature regression.

## V. EXPERIMENTAL RESULTS

### A. Settings

Tasks encompassing various levels are utilized to assess the versatility of the decoded feature sequence  $\{\hat{F}_t\}$ , specifically

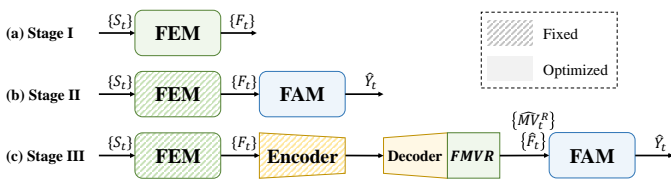


Fig. 7. Sketch for multi-stage training strategy. (a) Stage I: train the Feature Extraction Module. (b) Stage II: fix the Feature Extraction Module and train the Feature Analysis Module. (c) Stage III: fix the Feature Extraction Module and encoder and train the decoder, FMVR and Feature Analysis Module.

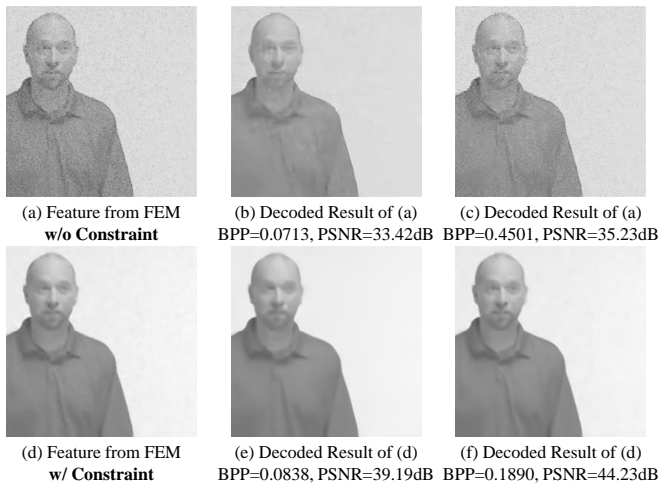


Fig. 8. Visual comparison between of the feature extracted from the spike sequence with and without constraint. (a) feature extracted from the Feature Extraction Module without constraint. (b~c) decoded results of (a) with different quantization steps. (d) feature extracted from the Feature Extraction Module with constraint. (e~f) decoded results of (d) with different quantization steps. Results show that the smoothness of feature plays a pivotal role in determining the codec’s efficiency. Zoom in for better visibility.

focusing on **scene reconstruction** and **classification** tasks. In the context of scene reconstruction, rich structural and textural details are acquired to ensure high pixel-level fidelity [38], which is evaluated on artificial *S-VIMEO*. In contrast, classification highlights the capability to extract high-level semantic information [39]. This is assessed on *S-MNIST*, *S-CIFAR*, and *S-CALTECH* referred to [11]. The ventral filter consists of 4 sub-filters with temporal receptive fields (TRFs) spreading from center towards both ends (TRF=7/9/11/13). The dorsal filter consists of 4 sub-filters with a fixed window size sliding backward (window\_size=10). Extensive experimental results showcase the exceptional performance of our model across both tasks.

### B. Training Strategy

The complexity of our model, with its numerous modules, poses a challenge for a unified training approach, as this might impede convergence and lead to poor performance. To address this, we advocate for a multi-stage training strategy, illustrating in Fig. 7. In the initial phase, we focus solely on training the Feature Extraction Module (FEM), as shown in Fig. 7(a). The objective here is to regulate the network’s output to ensure the smoothness of the feature  $F_t$ , the importance of which will be elucidated subsequently. During the second

	w/o constraint	w/ constraint
L1-Norm of $\mathbb{O}\mathbb{P}_L$	0.1079	0.0090
L2-Norm of $\mathbb{O}\mathbb{P}_L$	0.0341	0.0003

TABLE II  
L1- AND L2-NORMS OF THE LAPLACE OPERATION. RESULTS SUBSTANTIATE THE LAPLACIAN OPERATOR’S EFFECTIVENESS IN ENHANCING SMOOTHNESS, AND REAFFIRM ITS UTILITY IN REFINING THE FEATURE REPRESENTATION FOR MORE EFFICIENT COMPRESSION.

phase, the FEM is fixed, and we train distinct Feature Analysis Modules (FAMs) for various tasks, as shown in Fig. 7(b). These modules are regressed using either the Mean Squared Error (MSE) loss for scene reconstruction or Cross-Entropy (CE) loss for classification to attain optimal performance. In the final stage, pre-trained codecs are integrated between the FEM and FAMs. While keeping the FEM and encoder fixed, we only fine-tune the decoder, FMVR and FAMs, as shown in Fig. 7(c). Empirical results demonstrate that this structured training approach not only makes the compressed bitstream suitable for various downstream applications but also significantly enhances performance across different tasks.

Although the intermediate feature  $F_t$  does not exert a direct influence on the loss function, its degree of smoothness plays a pivotal role in determining the codec’s efficiency. This further exerts a substantial influence on both the bit-rate and the efficacy of downstream intelligent tasks. Fig. 8 illustrates this concept by visualizing the features extracted from the spike sequence, thereby underscoring the criticality of imposing constraints on  $F_t$ . BPP and PSNR are acronyms for Bit Per Pixel and Peak Signal-to-Noise Ratio. In Fig. 8(a), where  $F_t$  remains unconstrained, the resultant high-frequency noise pervading the background not only fails to contribute positively to the final task performance but also detrimentally affects the codec’s functionality. Fig. 8(b~c) demonstrates that in the absence of constraints, the codec escalates the bit rate ineffectively, primarily to restore high-frequency noise. In stark contrast, Fig. 8(d) reveals that constraining  $F_t$  leads to a more uniform background, facilitating easier compression. Such a constraint enables the codec to prioritize the restoration of content-related high-frequency textures, which, as the bit rate escalates, results in an enhanced recovery of details, as vividly depicted in Fig. 8(e~f). Additionally, we have graphed the Rate-Distortion curves under both constrained and unconstrained scenarios, as depicted in the Fig. 9(c). The results reveal that, under constraints, the encoder exhibits superior bit-efficiency and reconstruction quality. This further corroborates the notion that smoother features are more amenable to compression. These findings highlight the effectiveness of applying constraints in enhancing the overall performance of the encoding process, particularly in terms of balancing the trade-off between bit rate and the fidelity of decoding.

For further evaluation, we employed the L1- and L2-Norms of the Laplacian operator ( $\mathbb{O}\mathbb{P}_L$ ) to quantify the smoothness of  $F_t$ , shown in Fig. 9. In the realm of image processing, the Laplacian operator is utilized to compute the second-order derivatives of pixel in both horizontal and vertical directions,

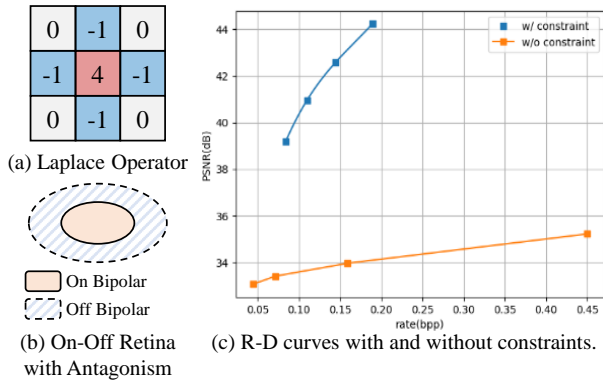


Fig. 9. (a) Sketch for the Laplacian operator. (b) Sketch for the On-Off retina with antagonism. The substantial similarity observed between these two structures validates the rationale behind employing Laplacian operator constraints to ensure feature smoothness. (c) Rate-distortion curve for methods with and without constraint.

facilitating the extraction of high-frequency content such as edge textures (Fig. 9(a)). This approach mirrors processes observed in biological vision systems, where ganglion cells, while integrating visual signals from bipolar cells, introduce an antagonistic mechanism to reduce redundancy in the optic nerve (Fig. 9(b)). This antagonism is typically represented by the Difference of Gaussian receptive fields (DoGs), akin to an isotropic Laplacian operator in its distribution. This analogy underscores that employing Laplacian operator-based constraints can effectively eliminate redundant high-frequency noise, thereby enhancing the compressibility of  $F_t$ . As indicated in Table II, the L1- and L2-Norms of the Laplacian operation for the constrained features exhibit a significant reduction. This not only substantiates the Laplacian operator’s effectiveness in enhancing smoothness but also reaffirms its utility in refining the feature representation for more efficient compression.

### C. Reconstruction Oriented Compression

To facilitate a comprehensive comparison of subjective quality, we depict the reconstructed scenes using different paradigms via various codecs, as shown in Fig. 10. For the *CTA* paradigm, the limited spatio-temporal continuity within spike sequences leads to pronounced blocking artifacts in the reconstruction, resulting in suboptimal reconstructed outcomes. For the *ATC* paradigm, distortions present in the reconstructed result from raw spikes are further accumulated and magnified with subsequent compression. In contrast, the *CAAS* paradigm enables approaches to simultaneously achieve minimal bit rates and distortion from raw spikes, resulting in superior performance compared to other methods.

**Rate-distortion loss.** To evaluate objective performance, we compute the PSNR between the ground truth and the scene reconstructed with different paradigms via variable codecs. The performance of approaches with the *ATC* and *CAAS* paradigms is indicated via Rate-Distortion curves shown in Fig. 11. It is observed from the curves that our method demonstrates significantly better compression efficiency and reduced reconstruction distortion across all bit rates. Furthermore, the

CTA Paradigm via						
DCVC		DCVC-DC		VTM		
BPP	PSNR	BPP	PSNR	QP	BPP	PSNR
0.60	13.29	<u>1.25</u>	19.31	40	0.13	12.2
<u>1.00</u>	14.42	<u>1.55</u>	19.43	42	0.56	16.9
<u>1.32</u>	15.04	<u>1.83</u>	19.51	44	0.63	17.42
<u>1.70</u>	15.50	<u>2.11</u>	19.69	46	<u>1.32</u>	20.36

TABLE III  
RATE-DISTORTION PERFORMANCE FOR *CTA* PARADIGM VIA VTM, DCVC AND DCVC-DC. THE UNDERLINE VALUES INDICATE THE REQUIREMENT OF COMPRESSION IS NOT ACCOMPLISHED, FOR BIT-RATE OF RAW SPIKE SEQUENCES IS 1 BPP.

	VTM [41]	DCVC [20]	DCVC-DC [21]
<b>Ours</b>	<b>-36.50%</b>	<b>-63.38%</b>	<b>-17.25%</b>

TABLE IV  
BD-RATE REDUCTION BETWEEN OUR METHOD AND OTHER APPROACHES WITH *CAAS* PARADIGM. NEGATIVE VALUES REPRESENT GAIN WHILE POSITIVE VALUES REPRESENT LOSS.

results also underscore the superiority of our proposed *CAAS* paradigm. Employing the same codec, the *CAAS* paradigm exhibits enhanced performance compared to the *ATC* paradigm, laying the groundwork for future research. Specific BD-rate [40] reductions are presented in Table IV, illustrating that our method outperforms other approaches by at least 17.25

The implications of employing the *CTA* paradigm are detailed in Table III. The underlined values indicate that the compression objectives are unmet, given that the bit rate of raw spike sequences stands at 1 BPP. Navigating the simultaneous optimization of bit rate and decoding quality poses a formidable challenge within the *CTA* paradigm, particularly in the context of standard bit-rate ranges. This challenge is primarily attributed to the inherent binary characteristic of spike sequences, which results in diminished spatio-temporal continuity and consequently leads to volatile reference relationship dynamics in both spatial and temporal dimensions.

To further illuminate this phenomenon, we showcase visualizations of the decoded outcomes utilizing the *CTA* paradigm via VTM, as depicted in Fig. 13. It becomes evident, particularly with increasing QP values, that the encoder progressively disregards spikes within areas of sparse population, as evidenced in Fig. 13(f~g). Additionally, pronounced block artifacts are observed in the decoded spike sequences, exemplified in Fig. 13(h), which significantly compromise information fidelity. Given the critical reliance of many spike-based intelligent applications on the precise timing of spike occurrences, such high distortion in the decoded spikes substantially hampers the efficacy of downstream tasks. The adverse effects of this distortion are further accentuated by the emergence of noise and discontinuities in the reconstructed scenarios, as illustrated in Fig. 13(j~l).

**Image quality assessment.** We employ non-reference Image Quality Assessment (IQA) metrics to evaluate the subjective quality, aligning with human perception [42]. Sev-

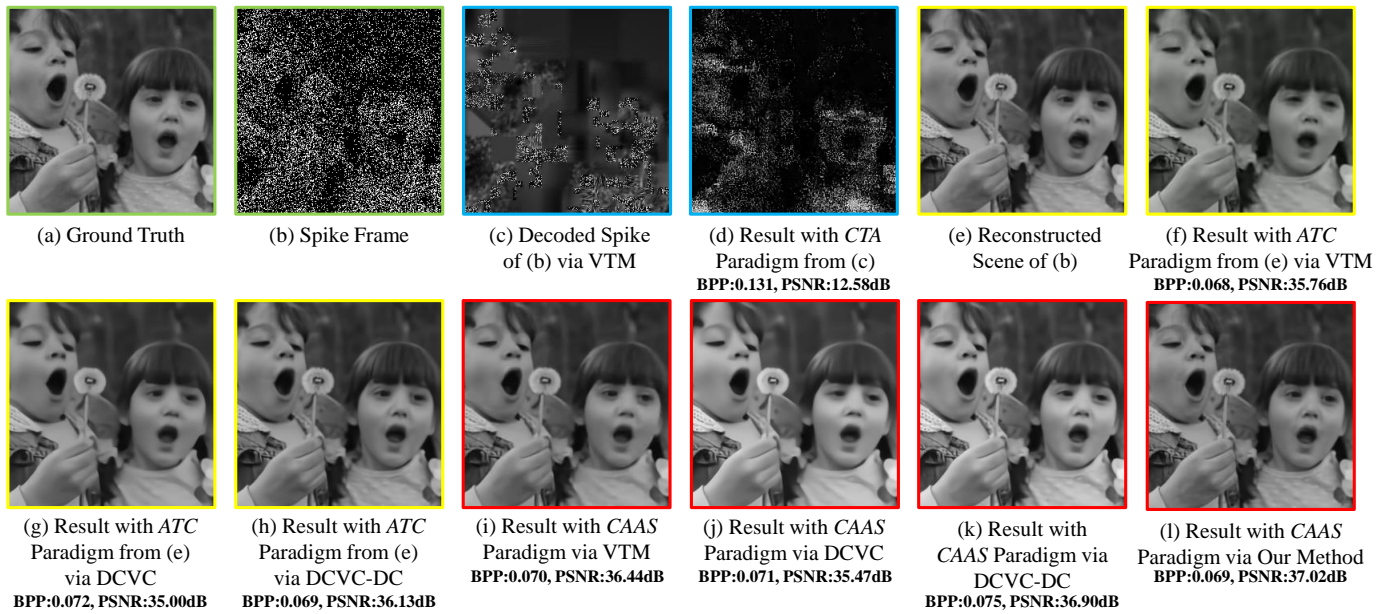


Fig. 10. Visualization for (a) ground truth, (b) spike frame, (c) decoded spike frame from (b) via VTM, (d) reconstructed scene from (c), (e) reconstructed scene from (b), (f~h) decoded scene from (e) via VTM, DCVC and DCVC-DC, (i~l) decoded and reconstructed scene from (b) via VTM, DCVC, DCVC-DC and our method. Subjective results show our method outperforms other approaches with CTA, ATC and CAAS paradigms, establishing a strong baseline. Zoom in for better visibility.

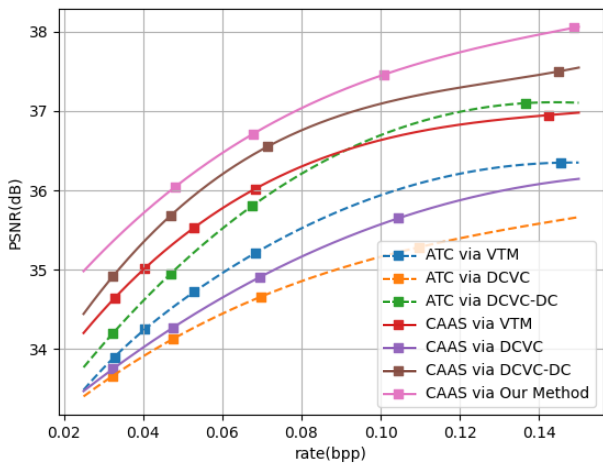


Fig. 11. Rate-distortion curve for approaches with ATC and CAAS paradigm. BPP is short for bit-per-pixel. Results illustrate that performance of our method exceeds that of all other approaches significantly, achieving 17.25% BD-rate reduction.

eral IQA metrics, including NIQE [43], MUSIQ [44], and BRISQUE [45], are selected for comprehensive analysis, with results presented in Table V. Our method achieves optimal performance across all metrics, demonstrating significant improvements over other approaches in terms of human perception. Simultaneously, this underscores the rationality and effectiveness of drawing inspiration from the mammalian vision system.

#### D. Classification Oriented Compression

We conduct thorough evaluations across all datasets to affirm the superiority of our methodologies. Notably, our

IQA Metric	CAAS Paradigm via			
	VTM	DCVC	DCVC-DC	Ours
<b>NIQE</b> [43] ( $\downarrow$ )	9.71	10.18	8.11	<b>7.71</b>
<b>MUSIQ</b> [44] ( $\uparrow$ )	32.58	31.61	39.19	<b>39.84</b>
<b>BRISQUE</b> [45] ( $\downarrow$ )	50.34	53.25	50.32	<b>49.54</b>

TABLE V  
THE IQA PERFORMANCE COMPARISON BETWEEN APPROACHES WITH CAAS PARADIGM VIA VTM, DCVC, DCVC-DC AND OUR METHOD. ( $\uparrow$ ) AND ( $\downarrow$ ) REPRESENT GREATER VALUE IS BETTER AND CONTRARY. RESULTS INDICATE OUR METHOD ACHIEVES OPTIMAL ON ALL METRICS.

method’s classification accuracy significantly surpasses that of the SOTA approach [11] when compression is not considered, as evidenced in Table VI. This underscores our method’s potential for maintaining high accuracy after compression, consistent with the experimental findings presented in Table VII. It is important to note that the anchor Bits Per Pixel (BPP) is set at 1, since transmitting a single spike incurs a cost of 1 bit, with the anchor accuracy detailed in Table VI. We observe a marginal decrease in accuracy (less than 20% in most instances), while achieving a significant reduction in transmission bits, exceeding 95% in savings. Furthermore, we employ the t-Distributed Stochastic Neighbor Embedding (t-SNE) technique [46] to reduce the dimensionality of predicted labels and visualize the outcomes, as depicted in Fig. 14. Despite the compression, predicted labels for samples within the same category remain tightly clustered in the high-dimensional space, thereby ensuring high fidelity in classification accuracy.

We present the classification report for the *S-MNIST* dataset, as showcased in the Table VIII. For simple characters such as 0, 5, and 7, our method demonstrates exceptional classifica-



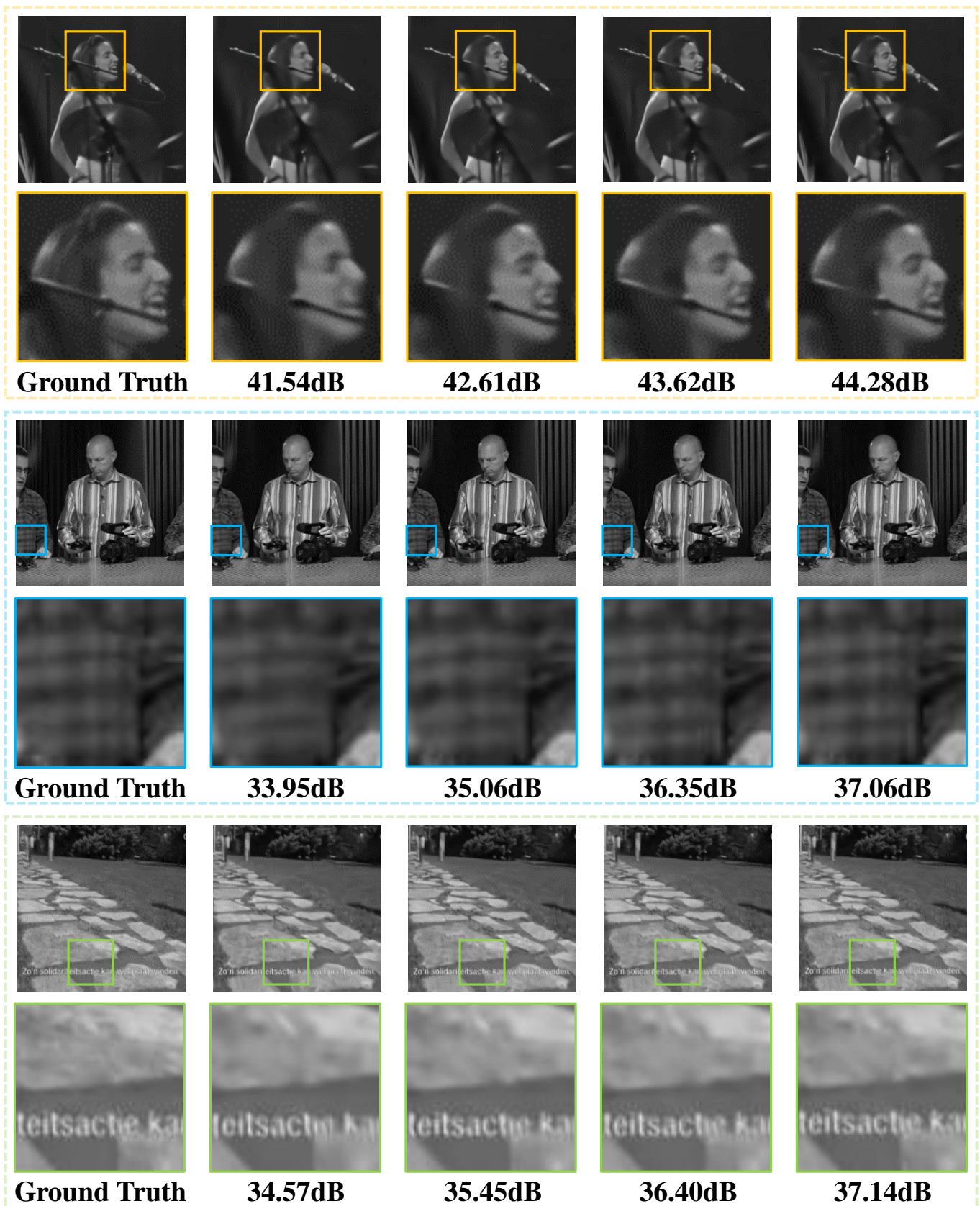


Fig. 12. Visualization of decoded and reconstructed scenes for simple scenarios. The first two rows, middle two rows and last two rows are selected from sequence 00001-0410, 00001-0330 and 00001-0160 respectively. The first column is ground truth, while the last four columns are decoded and reconstructed results with average bit-rate of 0.048, 0.068, 0.101, 0.149 BPP.

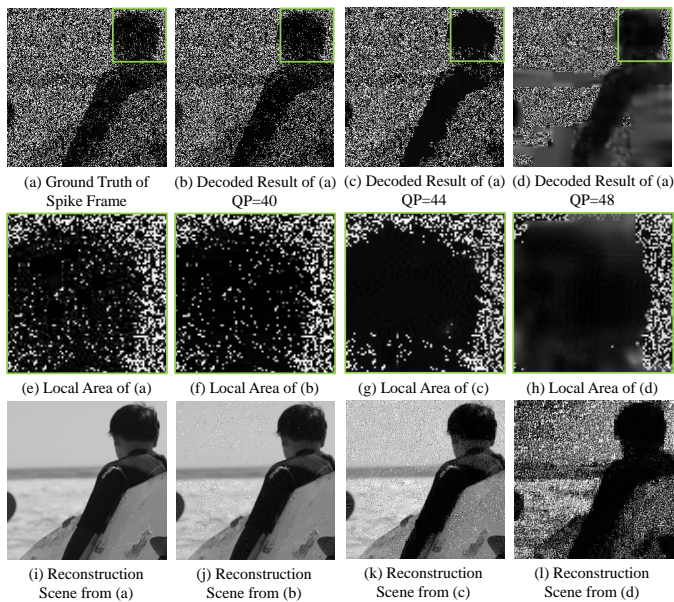


Fig. 13. Visual comparison of decoded spike frames via VTM with different QP and their reconstructed scenes. (a) ground truth of spike frame. (b~d) decoded results via VTM with QP=40, 44 and 48. (e~h) local area of (a~d). (i~l) reconstruction scenes from (a~d). Results indicate that the inherent binary characteristic of spike sequence culminates in diminished spatio-temporal continuity, leading to severe distortion for compression and downstream intelligent applications. Zoom in for better visibility.

Type	Method	Accuracy(%)		
		S-MNIST	S-CIFAR	S-CALTECH
Event	EtoF [47]	97.3	58.5	74.3
	BEI [48]	89.6	36.7	51.8
	SBNE [49]	96.2	56.4	73.8
Spike	SpiReco [11]	99.1	66.7	73.1
	<b>Ours</b>	<b>99.6</b>	<b>69.2</b>	<b>77.4</b>

TABLE VI

COMPARISON OF CLASSIFICATION ACCURACY BETWEEN SOTA APPROACHES FOR EVENT AND SPIKE DATA, AND OUR METHOD. ACCURACY OF OTHER APPROACHES IS OBTAINED FROM [11]. RESULTS SHOW THAT OUR METHOD FAR EXCEEDS OTHER APPROACHES, PROVIDING SUPPORT FOR FIDELITY AFTER COMPRESSION.

Dataset	BPP	0.011	0.016	0.025	0.038
<b>S-MNIST</b>	BS(%)	99.00	98.56	97.79	96.65
	AD(%)	13.2	12.0	11.6	10.8
<b>S-CIFAR</b>	BS(%)	98.76	98.18	97.14	95.66
	AD(%)	16.3	13.9	13.5	13.1
<b>S-CALTECH</b>	BS(%)	98.91	98.41	97.53	96.25
	AD(%)	9.3	7.9	7.4	6.7

TABLE VII

BENEFITS OF INTRODUCING COMPRESSION TO CLASSIFICATION TASKS.

COMPARISONS ARE ACCOMPLISHED IN BIT-SAVING (BS) AND ACCURACY-DECREASING (AD) PERFORMANCE BETWEEN OUR METHOD ON MNIST, CIFAR AND CALTECH DATASET. RESULTS SHOW THAT CLASSIFICATION ACCURACY DECREASES SLIGHTLY, WHILE BIT SAVING IS SIGNIFICANT, EXCEEDING 95%.

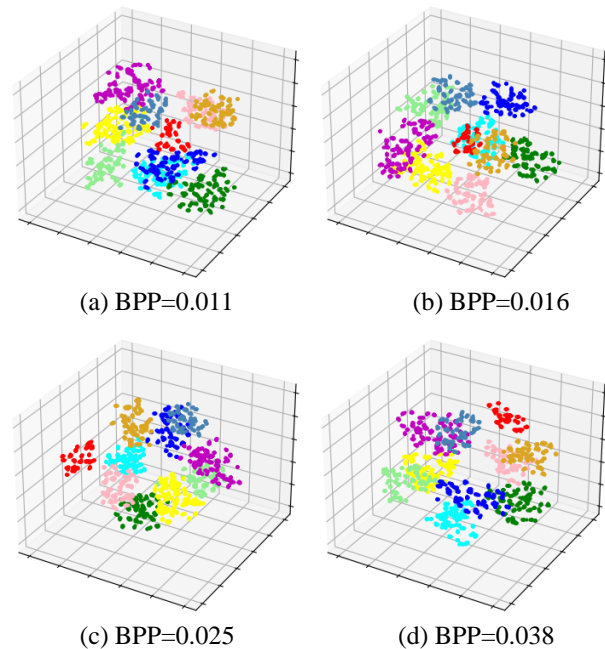


Fig. 14. Visualization of category aggregation within dataset S-MNIST after compression with various BPP. Despite being compressed, results show that samples of the same category are still largely clustered together, leading to high accuracy for classification.

Category	Precision	Recall	F1-Score
0	0.9883	0.9817	0.9849
1	0.9826	0.9883	0.9855
2	0.9818	0.9892	0.9855
3	0.9777	0.9850	0.9813
4	0.9617	0.9833	0.9724
5	0.9957	0.9642	0.9797
6	0.9693	0.9750	0.9722
7	0.9974	0.9592	0.9779
8	0.9529	0.9608	0.9568
9	0.9313	0.9492	0.9402
<b>Accuracy</b>	0.9736		
<b>Macro Avg</b>	0.9739	0.9736	0.9736
<b>Weighted Avg</b>	0.9739	0.9736	0.9736

TABLE VIII

THE CLASSIFICATION REPORT FOR S-MNIST DATASET. RESULTS SHOW THAT OUR METHOD DEMONSTRATES EXCEPTIONAL CLASSIFICATION ACCURACY FOR SIMPLE CHARACTERS, WHILE EXHIBITING A TENDENCY TO ERRONEOUSLY CATEGORIZE FOR COMPLEX ONES.

tion accuracy. However, it encounters challenges with more complex characters like 6, 8, and 9. In these cases, the model exhibits a tendency to erroneously categorize them as negative instances, leading to inaccuracies in the classification. This pattern suggests the need for further refinement in the model's ability to differentiate between characters with intricate features, underscoring an area for potential improvement in our approach.

E. Ablation Study

We design experiments to illustrate the effectiveness of three technical contributions by visualizing results and features, including dual-pathway structure, FMVR and AFR.

**Dual-pathway supervised structure.** The conventional single-pathway structure excels in capturing structural information for low-speed scenarios, enabling high quality scene reconstruction. However, it struggles to handle blur artifact caused by high-speed movement, which is shown in Fig. 15(a) and (b). The proposed dual-pathway supervised structure adaptively captures motion characteristic, eliminating blur and discontinuity effect, which is shown in Fig. 15(c) and (d). For scenarios with high-speed movement, the dorsal pathway extracts motion information such as direction and velocity, supervising the refinement of structural content through PFU. Results indicate that the method exhibits a greater gain in reconstructing high-speed scenes (2.11dB) compared to low-speed ones (1.36dB). By comparing Fig. 15(f) and (h), it is learned that our proposed dual-pathway supervised structure can effectively reduce the deviation of overall light intensity within frame, enhancing the quality of reconstructed scene. As for Fig. 15(e) and (g), it can be observed that blur located in edge areas is also significantly eliminated. Compared with ventral pathway only, the dual-pathway architecture improves PSNR results by **1.62dB** in average, demonstrating its effectiveness in handling spatial-temporal coupling information.

**FMVR.** The warping operation in codec is performed in latent domain, making motion vectors similar with latents rather than features. It is observed that intensity is not uniformly distributed in regions containing rich textures, such as background area of Fig. 16(a). This results in Moire artifact within the content, as illustrated in Fig. 16(c). To ensure the consistency between motion vectors and features for more precise warping, we refine the motion vectors based on the content of features. The result shown in Fig. 16(d) indicates that refined motion vector has eliminated texture and is similar with feature content. Through our proposed FMVR, the motion dynamic of distinct regions is enhanced such that Moire artifact is reduced. Regarding the reconstructed scene, the contextual content can be effectively aligned, which provides support for eliminating the ambiguity for intelligent tasks. The proposed FMVR module increases **1.22**, **0.03** and **0.01** for MUSIQ, DBCNN and CNNIQA respectively, indicating strong constraints on optical flow and feature content.

**AFR.** Due to the limitation of receptive field, single DCN can only handle sub-pixel level offsets. Large-scale movement can be addressed by employing upsampling, as well as stacking hierarchical levels of DCN. However, low-resolution offsets may introduce pixel-level inaccuracies when upsampled to high resolution. This exceeds the processing capacity of DCN, resulting in pixel-level discontinuities after alignment which is shown in Fig. 17(b). We propose AFR to address this issue, using motion vector to represent large-scale movement. Warped with refined motion vector, scene can be essentially rebuilt, as illustrated in Fig. 17(c), which means motions with large-scale are well considered. This allows DCN to focus on capturing small-scale movement by capitalizing advantages in

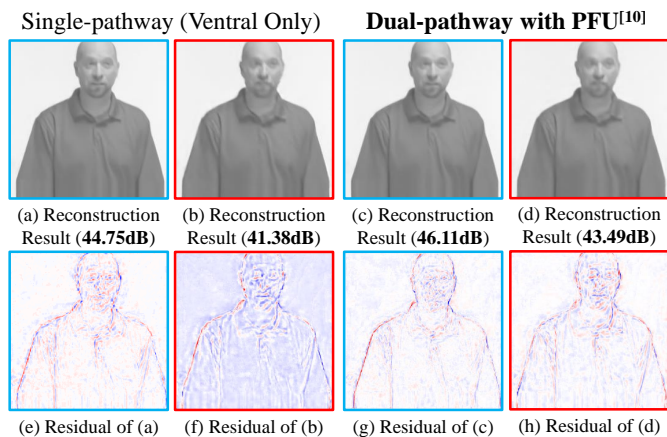


Fig. 15. Visual comparison between reconstructed scenes via single- and dual-pathway structure. Blue borders for low-speed scenarios and red borders for high-speed ones. Results show that dual-pathway structure and PFU exhibit greater gain for high-speed scenarios (2.11dB) compared to low-speed ones (1.36dB). Zoom in for better visibility.

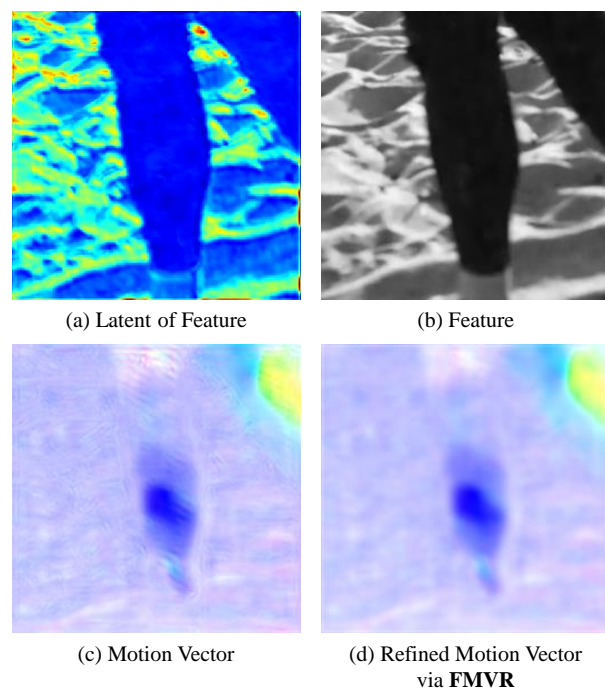


Fig. 16. Visualization for (a) latent of feature, (b) feature, (c) motion vector and (d) refined motion vector. Results show FMVR eliminates molecular pattern which is discrete with feature content, supporting for precise alignment.

sub-pixel perception and generate precise offsets. After fusing results from warping and deformation, the regressed feature exhibits smoother transitions and leads to more accurate scene reconstruction, showing in Fig. 17(d). For non-reference assessments, metrics of method with AFR decreases **1.41**, **23.18** and **0.62** for NIQE, ILNIQE and PI respectively compared those of baseline, demonstrating its effectiveness in handling spatial-temporal coupling information.

F. Complexity Analysis

In order to thoroughly assess the impact of the three technical innovations we have proposed, we conduct a detailed com-

Technical Contribution	Approaches for Comparison	Flops	Parameters	Inference Time
<b>Dual-pathway and PFU (End-Side)</b>	Extraction Module with Ventral Pathway Only	73.09G	1.11M	31.44ms
	Extraction Module with Dual-pathway and PFU <sup>[10]</sup>	74.79G	1.24M	35.01ms
	Increase	<b>2.33%</b>	<b>11.7%</b>	<b>11.35%</b>
<b>FMVR (End- &amp; Cloud-Side)</b>	Codec without FMVR	585.55G	21.96M	76.39ms
	Codec with FMVR	585.85G	21.97M	77.58ms
	Increase	<b>0.05%</b>	<b>0.04%</b>	<b>1.56%</b>
<b>AFR (Cloud-Side)</b>	Analysis Module with DCN-based Alignment Only	288.30G	2.65M	44.74ms
	Analysis Module with AFR	464.77G	3.32M	48.16ms
	Increase	<b>61.21%</b>	<b>25.28%</b>	<b>7.64%</b>

TABLE IX

COMPUTATIONAL CONSUMPTION COMPARISON OF TECHNICAL CONTRIBUTIONS WE PROPOSED, INCLUDING THE DUAL-PATHWAY AND PFU, FMVR AND AFR. RESULTS OUR TECHNICAL CONTRIBUTIONS DOES NOT SIGNIFICANTLY INCREASE THE COMPLEXITY AND PARAMETERS AT THE END-SIDE (2.33% AND 11.7%), WHILE ENHANCING FEATURE EXTRACTION PERFORMANCE AND SPIKE COMPRESSION EFFICIENCY.

	SpikeCodec [14]			Ours		
	Complexity (GFlops)	Parameter (M)	Inference Time (ms)	Complexity (GFlops)	Parameter (M)	Inference Time (ms)
<b>I-enc</b>	679.40	6.11	155.57	<b>79.76</b>	<b>6.03</b>	<b>89.60</b>
<b>P-enc</b>	-	-	-	<b>96.13</b>	<b>3.90</b>	<b>110.32</b>
<b>I-dec</b>	18.28	42.88	60.59	457.96	27.90	89.86
<b>P-dec</b>	-	-	-	489.42	18.06	97.67

TABLE X

COMPARISON OF COMPUTATIONAL CONSUMPTION BETWEEN SPIKECODEC [14] AND OUR METHOD. RESULTS INDICATE THAT OVERHEAD FOR ENCODER IS REDUCED SIGNIFICANTLY (88.26%), PROVIDING SUPPORT FOR SPIKE ENCODING ON LOW-POWER AND EMBEDDED DEVICES.

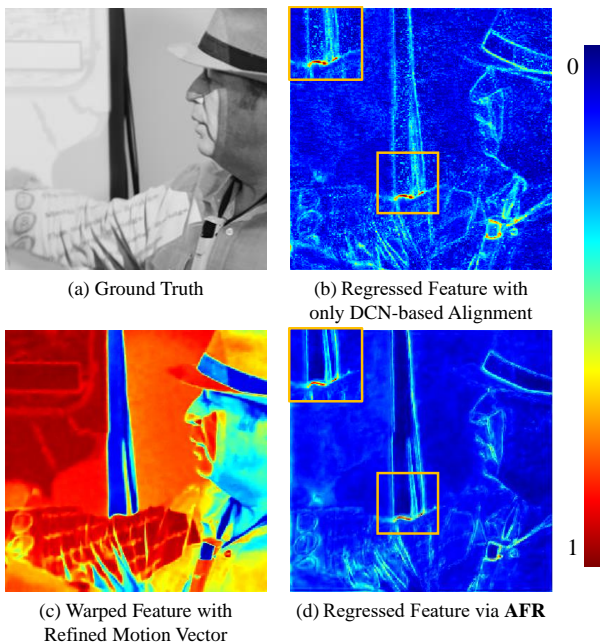


Fig. 17. Visualization for (a) ground truth, (b) regressed feature with only PCD alignment, (c) warped feature with refined motion vector and (d) regressed feature with AFR. Results show that pixel-level inaccuracies are reduced and aligned feature exhibits smoother with assistance of warp-based alignment, leading to more accurate reconstructed scene.

parison of the increases in complexity and parameters, which is systematically presented in Table IX<sup>1</sup>. The results demonstrate that the dual-pathway architecture with PFU does not significantly increase the complexity and parameters (2.33% and 11.7%), while enhancing feature extraction performance and spike compression efficiency. On the other hand, while there is a notable increase in both complexity and parameters for AFR (61.21% and 25.28%), the inference time can be effectively reduced through parallel optimization techniques (only 7.64% increase), leveraging concurrent processing capabilities and allowing for more efficient execution of computational tasks.

Since our framework is designed for the end-cloud collaborative environment, we further compare complexity and parameters of encoder (end-side) and decoder (cloud-side) between our method and SpikeCodec, which is the SOTA approach for reconstruction based spike compression, as shown in Table X.<sup>2</sup> Our scheme dramatically reduces computational consumption required for encoder, especially for complexity (88.26%), which provides support for spike encoding on low-power and embedded devices [50] [51]. Despite the high overhead of decoder, the hardware resources in the cloud-side

<sup>1</sup>The inference time is evaluated on Intel(R) i7-7700 @ 3.60GHz CPU and Geforce RTX 3080 GPU with input resolution of 256 × 256.

<sup>2</sup>The inference time is evaluated on NVIDIA Geforce RTX 3080 and 4090 GPU for encoding and decoding respectively, simulating the computational difference between end-side and cloud-side.

are fully affordable in end-cloud collaboration architecture, enabling real-time decoding and analysis. This clearly illustrates the superiority of our approach within the end-cloud collaborative framework, striking an effective balance between computational efficiency and performance enhancement. Our method significantly contributes to the popularization of spike cameras and spike-based applications.

It's worth mentioning that, the analysis model deployed at the cloud-side can be adjusted for different tasks, and the model size can also be adapted according to granularity and precision requirements, demonstrating the generality, flexibility, and robustness of our approach. Future research endeavors should concentrate on two key aspects. Firstly, enhancing the parallel processing capabilities of the feature extraction module is crucial. This improvement aims to reduce inference time, thereby enabling real-time feature extraction and compression. Secondly, it is imperative to simplify the complexity of the analytical network, decreasing both the hardware requirements and the associated costs, making the technology more efficient. These focal points will collectively contribute to the development of more agile and cost-effective systems, suitable for a wider range of applications.

## VI. CONCLUSION

In this paper, we for the first time conceptualize the SCI, which jointly optimizes the low-level spike compression and high-level spike analysis. We propose a novel spike compression framework encapsulated with dual-pathway structure, advanced motion expression module and feature regression module. Our method realizes high efficiency spike compact representation and high performance spike reconstruction and classification with low computational resource consumption. Extensive experimental results show that our scheme obtains SOTA performance in both compression and analysis tasks. This research enables a novel sub-field for spike visual intelligence, facilitating future study.

## REFERENCES

- [1] Maxime Meilland, Tom Drummond, and Andrew I Comport. A unified rolling shutter and motion blur model for 3d visual registration. In *Proceedings of the IEEE International Conference on Computer Vision*, pages 2016–2023, 2013.
- [2] Michael Schöberl, Andreas Brückner, Siegfried Foessel, and André Kaup. Photometric limits for digital camera systems. *Journal of Electronic Imaging*, 21(2):020501–020501, 2012.
- [3] Martin Litzenberger, Christoph Posch, D Bauer, Ahmed Nabil Belbachir, P Schon, B Kohn, and H Garn. Embedded vision system for real-time object tracking using an asynchronous transient vision sensor. In *2006 IEEE 12th Digital Signal Processing Workshop & 4th IEEE Signal Processing Education Workshop*, pages 173–178, 2006.
- [4] Thomas B Moeslund, Adrian Hilton, and Volker Krüger. A survey of advances in vision-based human motion capture and analysis. *Computer Vision and Image Understanding*, 104(2-3):90–126, 2006.
- [5] Heinz Wassele and BRIAN B Boycott. Functional architecture of the mammalian retina. *Physiological reviews*, 71(2):447–480, 1991.
- [6] Andreas Bringmann, Steffen Syrbe, Katja Görner, Johannes Kacza, Mike Francke, Peter Wiedemann, and Andreas Reichenbach. The primate fovea: structure, function and development. *Progress in retinal and eye research*, 66:49–84, 2018.
- [7] JN Li and YH Tian. Recent advances in neuromorphic vision sensors: A survey. *Chinese Journal of Computers*, 44(6):1258–1286, 2021.
- [8] Yongqiang Zhang, Hongchang Yu, Wanzhen Zhou, and Menghua Man. Application and research of iot architecture for end-net-cloud edge computing. *Electronics*, 12(1):1, 2023.
- [9] Guoping Rong, Yangchen Xu, Xinxin Tong, and Haojun Fan. An edge-cloud collaborative computing platform for building aiot applications efficiently. *Journal of Cloud Computing*, 10:1–14, 2021.
- [10] Jing Zhao, Ruiqin Xiong, Hangfan Liu, Jian Zhang, and Tiejun Huang. Spk2imgnet: Learning to reconstruct dynamic scene from continuous spike stream. In *Proceedings of the IEEE/CVF Conference on Computer Vision and Pattern Recognition*, pages 11996–12005, 2021.
- [11] Junwei Zhao, Shiliang Zhang, Zhaofei Yu, and Tiejun Huang. Spireco: Fast and efficient recognition of high-speed moving objects with spike cameras. *IEEE Transactions on Circuits and Systems for Video Technology*, 2023.
- [12] Man Yao, Jiakui Hu, Zhaokun Zhou, Li Yuan, Yonghong Tian, Bo Xu, and Guoqi Li. Spike-driven transformer. *arXiv preprint arXiv:2307.01694*, 2023.
- [13] Siwei Dong, Zhichao Bi, Yonghong Tian, and Tiejun Huang. Spike coding for dynamic vision sensor in intelligent driving. *IEEE Internet of Things Journal*, 6(1):60–71, 2018.
- [14] Kexiang Feng, Chuanmin Jia, Siwei Ma, and Wen Gao. Spikecodec: An end-to-end learned compression framework for spiking camera. *arXiv preprint arXiv:2306.14108*, 2023.
- [15] Fanke Dong and Chuanmin Jia. Learned lossless coding for ultra-high-speed spike streams via intensity remapping. In *2024 IEEE International Conference on Visual Communications and Image Processing (VCIP)*, pages 1–5. IEEE, 2024.
- [16] Wenhong Duan, Zheng Chang, Chuanmin Jia, Shanshe Wang, Siwei Ma, Li Song, and Wen Gao. Learned image compression using cross-component attention mechanism. *IEEE Transactions on Image Processing*, 32:5478–5493, 2023.
- [17] Chuanmin Jia, Xinyu Hang, Shanshe Wang, Yaqiang Wu, Siwei Ma, and Wen Gao. Fpx-nic: An fpga-accelerated 4k ultra-high-definition neural video coding system. *IEEE Transactions on Circuits and Systems for Video Technology*, 32(9):6385–6399, 2022.
- [18] Siwei Ma, Xinfeng Zhang, Chuanmin Jia, Zhenghui Zhao, Shiqi Wang, and Shanshe Wang. Image and video compression with neural networks: A review. *IEEE Transactions on Circuits and Systems for Video Technology*, 30(6):1683–1698, 2019.
- [19] Guo Lu, Wanli Ouyang, Dong Xu, Xiaoyun Zhang, Chunlei Cai, and Zhiyong Gao. Dvc: An end-to-end deep video compression framework. In *Proceedings of the IEEE/CVF Conference on Computer Vision and Pattern Recognition*, pages 11006–11015, 2019.
- [20] Jiahao Li, Bin Li, and Yan Lu. Deep contextual video compression. *Advances in Neural Information Processing Systems*, 34:18114–18125, 2021.
- [21] Jiahao Li, Bin Li, and Yan Lu. Neural video compression with diverse contexts. In *Proceedings of the IEEE/CVF Conference on Computer Vision and Pattern Recognition*, pages 22616–22626, 2023.
- [22] Wenhan Yang, Haofeng Huang, Yueyu Hu, Ling-Yu Duan, and Jiaying Liu. Video coding for machine: Compact visual representation compression for intelligent collaborative analytics. *arXiv preprint arXiv:2110.09241*, 2021.
- [23] Kristian Fischer, Fabian Brand, Christian Herglotz, and André Kaup. Video coding for machines with feature-based rate-distortion optimization. In *2020 IEEE 22nd International Workshop on Multimedia Signal Processing (MMSP)*, pages 1–6. IEEE, 2020.
- [24] Dwight J Kravitz, Kadharbata S Saleem, Chris I Baker, and Mortimer Mishkin. A new neural framework for visuospatial processing. *Nature Reviews Neuroscience*, 12(4):217–230, 2011.
- [25] A David Milner and Melvyn A Goodale. Two visual systems re-viewed. *Neuropsychologia*, 46(3):774–785, 2008.
- [26] Ashish Vaswani, Noam Shazeer, Niki Parmar, Jakob Uszkoreit, Llion Jones, Aidan N Gomez, Łukasz Kaiser, and Illia Polosukhin. Attention is all you need. *Advances in neural information processing systems*, 30, 2017.
- [27] Vonne Van Polanen and Marco Davare. Interactions between dorsal and ventral streams for controlling skilled grasp. *Neuropsychologia*, 79:186–191, 2015.
- [28] Vladislav Ayzenberg, Claire Simmons, and Marlene Behrmann. Temporal asymmetries and interactions between dorsal and ventral visual pathways during object recognition. *Cerebral Cortex Communications*, 4(1):tgad003, 2023.
- [29] Ivan Skorokhodov, Grigorii Sotnikov, and Mohamed Elhoseiny. Aligning latent and image spaces to connect the unconnectable. In *Proceedings of the IEEE/CVF International Conference on Computer Vision*, pages 14144–14153, 2021.
- [30] Scznu \_ Me and Acquiltion v Pmcmn. Small convolution kernels for high-fidelity image restoration. *IEEE Transactions on Signal Processing*, 39(10):2253, 1991.

- [31] Thiemo Alldieck, Marc Kassubeck, Bastian Wandt, Bodo Rosenhahn, and Marcus Magnor. Optical flow-based 3d human motion estimation from monocular video. In *Pattern Recognition: 39th German Conference, GCPR 2017, Basel, Switzerland, September 12–15, 2017, Proceedings 39*, pages 347–360. Springer, 2017.
- [32] Thomas Brox and Jitendra Malik. Large displacement optical flow: descriptor matching in variational motion estimation. *IEEE transactions on pattern analysis and machine intelligence*, 33(3):500–513, 2010.
- [33] Xizhou Zhu, Han Hu, Stephen Lin, and Jifeng Dai. Deformable convnets v2: More deformable, better results. In *Proceedings of the IEEE/CVF conference on computer vision and pattern recognition*, pages 9308–9316, 2019.
- [34] Jifeng Dai, Haozhi Qi, Yuwen Xiong, Yi Li, Guodong Zhang, Han Hu, and Yichen Wei. Deformable convolutional networks. In *Proceedings of the IEEE international conference on computer vision*, pages 764–773, 2017.
- [35] Xintao Wang, Kelvin CK Chan, Ke Yu, Chao Dong, and Chen Change Loy. Edvr: Video restoration with enhanced deformable convolutional networks. In *Proceedings of the IEEE/CVF conference on computer vision and pattern recognition workshops*, pages 0–0, 2019.
- [36] Yulin Huang and Junying Chen. Improved edvr model for robust and efficient video super-resolution. In *Proceedings of the IEEE/CVF Winter Conference on Applications of Computer Vision*, pages 103–111, 2022.
- [37] Kelvin CK Chan, Xintao Wang, Ke Yu, Chao Dong, and Chen Change Loy. Understanding deformable alignment in video super-resolution. In *Proceedings of the AAAI conference on artificial intelligence*, volume 35, pages 973–981, 2021.
- [38] Sergey N Starikov, Nikita N Balan, Mikhail V Konnik, Vladislav G Rodin, Ivan V Solyakin, and Ekaterina A Shapkarina. Input scene restoration in pattern recognition correlator based on digital photo camera. In *Optical Pattern Recognition XVIII*, volume 6574, pages 181–190. SPIE, 2007.
- [39] Dengsheng Lu and Qihao Weng. A survey of image classification methods and techniques for improving classification performance. *International journal of Remote sensing*, 28(5):823–870, 2007.
- [40] Gisle Bjontegaard. Calculation of average psnr differences between rd-curves. *ITU SG16 Doc. VCEG-M33*, 2001.
- [41] Benjamin Bross, Ye-Kui Wang, Yan Ye, Shan Liu, Jianle Chen, Gary J Sullivan, and Jens-Rainer Ohm. Overview of the versatile video coding (vvc) standard and its applications. *IEEE Transactions on Circuits and Systems for Video Technology*, 31(10):3736–3764, 2021.
- [42] JE Ospina-Borras and HD Benitez-Restrepo. Non-reference quality assessment of infrared images reconstructed by compressive sensing. In *Image Quality and System Performance XII*, volume 9396, pages 274–282. SPIE, 2015.
- [43] Anish Mittal, Rajiv Soundararajan, and Alan C Bovik. Making a “completely blind” image quality analyzer. *IEEE Signal processing letters*, 20(3):209–212, 2012.
- [44] Junjie Ke, Qifei Wang, Yilin Wang, Peyman Milanfar, and Feng Yang. Musicq: Multi-scale image quality transformer. In *Proceedings of the IEEE/CVF International Conference on Computer Vision*, pages 5148–5157, 2021.
- [45] Anish Mittal, Anush Krishna Moorthy, and Alan Conrad Bovik. No-reference image quality assessment in the spatial domain. *IEEE Transactions on image processing*, 21(12):4695–4708, 2012.
- [46] Laurens Van der Maaten and Geoffrey Hinton. Visualizing data using t-sne. *Journal of machine learning research*, 9(11), 2008.
- [47] Shafiq Ahmad, Gianluca Scarpellini, Pietro Morerio, and Alessio Del Bue. Event-driven re-id: A new benchmark and method towards privacy-preserving person re-identification. In *Proceedings of the IEEE/CVF Winter Conference on Applications of Computer Vision*, pages 459–468, 2022.
- [48] Gregory Cohen, Saeed Afshar, Garrick Orchard, Jonathan Tapson, Ryad Benosman, and Andre van Schaik. Spatial and temporal downsampling in event-based visual classification. *IEEE Transactions on Neural Networks and Learning Systems*, 29(10):5030–5044, 2018.
- [49] Kaixuan Zhang, Kaiwei Che, Jianguo Zhang, Jie Cheng, Ziyang Zhang, Qinghai Guo, and Luziwei Leng. Discrete time convolution for fast event-based stereo. In *Proceedings of the IEEE/CVF Conference on Computer Vision and Pattern Recognition*, pages 8676–8686, 2022.
- [50] Gautier Berthou, Kevin Marquet, Tanguy Risset, and Guillaume Salagnac. Accurate power consumption evaluation for peripherals in ultra low-power embedded systems. In *2020 Global Internet of Things Summit (GloTS)*, pages 1–6. IEEE, 2020.
- [51] Girma S Tewolde. Current trends in low-power embedded computing. In *2010 IEEE International Conference on Electro/Information Technology*, pages 1–6. IEEE, 2010.